Session II

Formation of Large-Scale Structure

https://doi.org/10.1017/S0074180900196524 Published online by Cambridge University Press

Maps of the Cosmos
ASP Conference Series, Vol. 216, 2005
M. Colless, L. Staveley-Smith, R. Stathakis

Large-Scale Structure from 2dFGRS

J. A. Peacock*

Institute for Astronomy, University of Edinburgh, Royal Observatory, Edinburgh EH9 3HJ, UK

Abstract. The 2dF Galaxy Redshift Survey is now complete, and the full data are public. 2dFGRS was the first survey to observe more than 100,000 redshifts, making possible precise measurements of many aspects of galaxy clustering, which can be studied as a function of galaxy spectral type, and also of broad-band colour. Early-type galaxies are more strongly clustered than late types, with a relative bias of $b = 1.25 \pm 0.09$ on large scales. For both types, luminosity dependence of clustering is detected at high significance, and is well described by a relative bias of $b/b^* = 0.85 + 0.15(L/L^*)$. This is consistent with the observation that L^* in rich clusters is brighter than the global value by 0.28 ± 0.08 mag. Redshift-space distortions from large-scale infall velocities measure the distortion parameter $\beta \equiv \Omega_m^{0.6}/b = 0.49 \pm 0.09$. The power spectrum is measured to $\lesssim 10\%$ accuracy for $k > 0.02\,h\,\mathrm{Mpc}^{-1}$, and is well fitted by a CDM model with $\Omega_m h = 0.18 \pm 0.02$ and a baryon fraction of 0.17 ± 0.06. The 2dFGRS plays an essential role in breaking model degeneracies inherent in CMB data; a joint analysis with WMAP results requires $\Omega_m = 0.25 \pm 15\%$ and $h = 0.73 \pm 5\%$, assuming scalar fluctuations.

1. Outline of the 2dFGRS Data

The 2dF Galaxy Redshift Survey (2dFGRS) has received frequent mention in the talks at this meeting, so it is appropriate to give a little more detail on this project. The survey used the two-degree field fibre-optic positioner and spectrograph on the AAT, which allows redshifts to be obtained for 400 objects over a circle of diameter 2 degrees, in about one hour integration time. For details of the instrument and its performance see `http://www.aao.gov.au/2df/`, and also Lewis et al. (2002).

The main period of 2dFGRS observing was between May 1997 and April 2002. In total, observations were made of 245 591 objects, yielding redshifts and identifications for 229 118 galaxies, 16348 stars and 125 QSOs. The galaxy redshifts are assigned a quality flag from 1 to 5, where the probability of er-

On behalf of the 2dF Galaxy Redshift Survey team: Matthew Colless (ANU), Ivan Baldry (JHU), Carlton Baugh (Durham), Joss Bland-Hawthorn (AAO), Terry Bridges (AAO), Russell Cannon (AAO), Shaun Cole (Durham), Chris Collins (LJMU), Warrick Couch (UNSW), Gavin Dalton (Oxford), Roberto De Propris (UNSW), Simon Driver (St Andrews), George Efstathiou (IoA), Richard Ellis (Caltech), Carlos Frenk (Durham), Karl Glazebrook (JHU), Carole Jackson (ANU), Ofer Lahav (IoA), Ian Lewis (AAO), Stuart Lumsden (Leeds), Steve Maddox (Nottingham), Darren Madgwick (IoA), Peder Norberg (Durham), Will Percival (ROE), Bruce Peterson (ANU), Will Sutherland (ROE), Keith Taylor (Caltech).

ror is highest at low Q. Most analyses are restricted to $Q \geq 3$ galaxies, of which there are 221 414. All spectra and redshifts are now public, and can be found at `http://www.mso.anu.edu.au/2dFGRS/Public`, together with software for manipulating the database. See Colless et al. (2001, 2003) for details of the survey.

The source catalogue for the survey is a revised and extended version of the APM galaxy catalogue (Maddox et al. 1990a,b; Maddox, Efstathiou, & Sutherland 1990c), which is based on Automated Plate Measuring machine (APM) scans of 390 plates from the UK Schmidt Telescope (UKST) Southern Sky Survey. The $b_{\rm J}$ magnitude system for the Southern Sky Survey is related to the Johnson–Cousins system by $b_{\rm J} = B - 0.304(B - V)$, where the colour term is estimated from comparison with the SDSS Early Data Release (Stoughton et al. 2002). The 2dFGRS target sample is limited to be brighter than an extinction-corrected magnitude of $b_{\rm J} = 19.45$ (using the extinction maps of Schlegel, Finkbeiner, & Davis 1998).

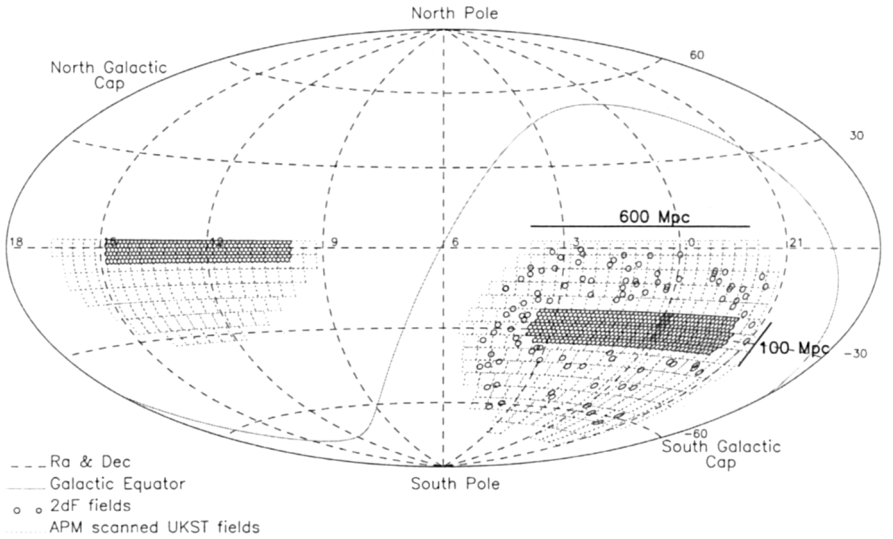

Figure 1. The 2dFGRS fields (small circles) superimposed on the APM catalogue area (dotted outlines of Sky Survey plates). There are approximately 140,000 galaxies in the 75° × 15° southern strip centred on the SGP, 70,000 galaxies in the 75° × 7.5° equatorial strip, and 40,000 galaxies in the 100 randomly-distributed 2dF fields covering the whole area of the APM catalogue in the south.

The survey geometry is shown in Figure 1, and consists of two contiguous declination strips, plus 100 random 2-degree fields. One strip is in the southern Galactic hemisphere and covers approximately 75°×15° centred close to the SGP at (α, δ)=$(01^h, -30°)$; the other strip is in the northern Galactic hemisphere and covers 75° × 7.5° centred at (α, δ)=$(12.5^h, +0°)$. The 100 random fields are spread uniformly over the 7000 deg^2 region of the APM catalogue in the southern Galactic hemisphere. At the median redshift of the survey ($\bar{z} = 0.11$),

https://doi.org/10.1017/S0074180900196524 Published online by Cambridge University Press

$100\,h^{-1}$ Mpc subtends about 20 degrees, so the two strips are $375\,h^{-1}$ Mpc long and have widths of $75\,h^{-1}$ Mpc (south) and $37.5\,h^{-1}$ Mpc (north).

The completed 2dFGRS yields a striking view of the galaxy distribution over large cosmological volumes. This is illustrated in Figure 2, which shows the projection of a subset of the galaxies in the northern and southern strips onto (α, z) slices. This picture is the culmination of decades of effort in the investigation of large-scale structure, and it allows us to study the statistical properties of the galaxies distribution with high precision, as described below.

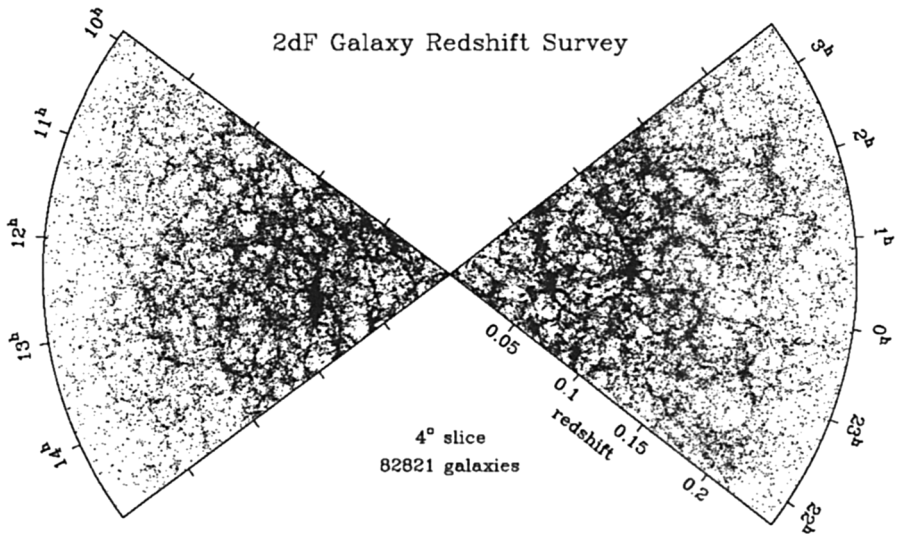

Figure 2. The distribution of galaxies in part of the 2dFGRS: slices 4° thick, centred at declination −2.5° in the NGP and −27.5° in the SGP. This magnificently detailed image of large-scale structure provides the basis for measuring the shape of the primordial fluctuation spectrum and hence constraining the matter content of the universe.

2. Galaxy Spectra and Colours

It is important on physical grounds to be able to divide the 2dFGRS database into different categories of galaxies. This has been done in two different ways. Spectral classification of 2dFGRS galaxies was performed by Folkes et al. (1999) and Madgwick et al. (2002). Principal component analysis was used to split galaxies into a superposition of a small number of templates. Not all of these are robust, owing to residual spectral distortions in the 2dF instrument, but it was possible to derive a robust classification parameter (termed η) from the templates, which effectively measures the emission-line strength (closely related to the star-formation rate). Galaxies were divided into four spectral classes; their mean spectra and separate luminosity functions are shown in Figure 3.

This classification method cannot be used beyond $z = 0.15$, where Hα is lost from the spectra. Also, the fibres do not cover the whole galaxy (although Madgwick et al. 2002 show that aperture corrections are not large in practice).

https://doi.org/10.1017/S0074180900196524 Published online by Cambridge University Press

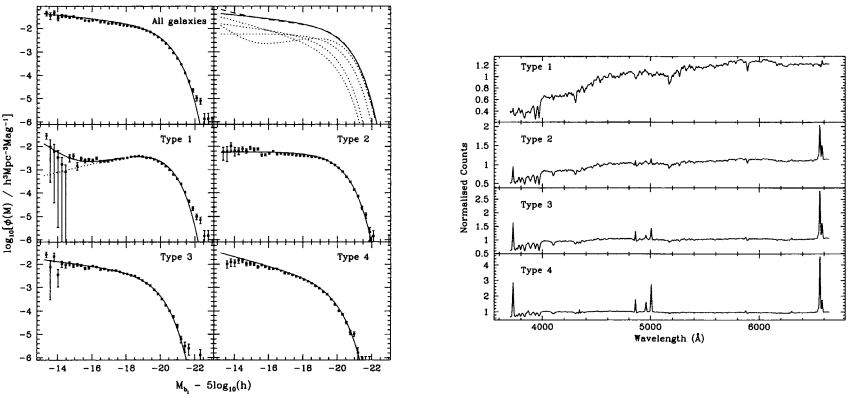

Figure 3. The type-dependent galaxy luminosity function according to Madgwick et al. (2002). Principal component analysis was used to split galaxies into a superposition of a small number of templates, and a categorization made based on the decomposition. Type 1 galaxies are generally E/S0, while later types range from Sa to Irr.

As an alternative, total broad-band colours have been derived for the 2dFGRS galaxies, using the data from the SuperCOSMOS sky surveys (Hambly, Irwin, & MacGillivray 2001). These yield B_J from the same UK Schmidt Plates as used in the original APM survey, but with improved linearity and smaller random errors (0.09 mag rms relative to the SDSS EDR data). The R_F plates are of similar quality, so that we are able to divide galaxies by colour, with an rms in photographic $B - R$ of about 0.13 mag. The systematic calibration uncertainties are negligible by comparison, and are at the level of 0.04 mag. rms in each band. Figure 4 shows that the colour information divides 'passive' or 'early-type' galaxies with little active star formation cleanly from the remainder, uniformly over the whole redshift range of the 2dFGRS.

3. Dependence of Clustering on Galaxy Type and Luminosity

In order to use galaxy clustering as a probe of the cosmic mass field, it is necessary to understand how and why the clustering signal varies with the class of galaxy under study. 2dFGRS has addressed this, first by studying the variation with luminosity (Norberg et al. 2001), and later looking at the full dependence on luminosity and on galaxy type (Norberg et al. 2002). These studies were carried out in real space, using the projected statistic $\Xi(\sigma) = \int \xi(\sigma, \pi)\, d\pi$.

The results (Figure 5) show that the clustering amplitude is an increasing function both of luminosity and of redness. The latter result, that early-type galaxies cluster more strongly than late types, is well established (e.g. Davis & Geller 1976), but the former was more controversial (Loveday et al. 1995; Benoist et al. 1996). A very clear detection of luminosity-dependent clustering was achieved, which can be described by a linear dependence of effective bias

https://doi.org/10.1017/S0074180900196524 Published online by Cambridge University Press

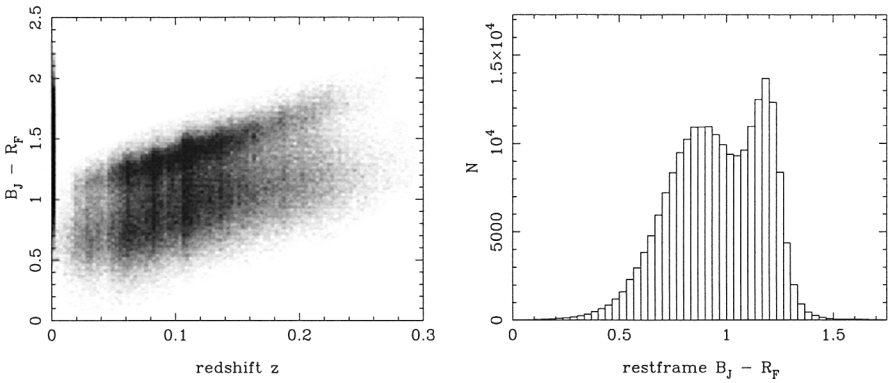

Figure 4. Photographic $B - R$ colour versus redshift for the 2dFGRS. The separation between 'early-type' (red) and 'late-type' (blue) galaxies is very clear. The second panel shows the histogram of K-corrected restframe colours, which is very clearly bimodal. This is strongly reminiscent of the distribution of the spectral type, η, and we assume that a division at $(B - R)_0 = 1.07$ achieves a separation of early-type 'class 1' galaxies from classes 2–4, as was done using spectra by Madgwick et al. (2002).

parameter on luminosity:

$$b/b^* = 0.85 + 0.15\,(L/L^*), \tag{1}$$

where L^* denotes the characteristic luminosity in the overall galaxy luminosity function, corresponding to $M_{B_J} = -19.66$ for $h = 1$. Nevertheless, at all luminosities there is a difference in the clustering properties of early-type and late-type galaxies. The relative bias may be defined via the ratio of the correlation functions:

$$b_{\rm rel} = [\xi_{\rm early}(r)/\xi_{\rm late}(r)]^{1/2} = 1.25 \pm 0.09, \tag{2}$$

where we choose a fiducial radius of $5\,h^{-1}$ Mpc. Of course, since late-type galaxies are bluer, this figure would decrease if the comparison were made at a constant R-band luminosity. The typical difference in rest $B - R$ is 0.5 mag, and this would reduce the relative bias by about a factor 1.1. This is reasonable from a theoretical point of view: since red light more nearly measures total stellar mass, this says that the principal cause of different clustering amplitudes is the mass of halo that hosts a galaxy (e.g. Cole & Kaiser 1989; Mo & White 1996; Kauffman, Nusser, & Steinmetz 1997).

Finally, these results would lead us to infer that the LF must change in strongly clumped regions, shifting to higher luminosities. Such an effect has been sought for many years, but always yielded null results. However, De Propris et al. (2003) have shown that L^* in rich clusters does obey a shift with respect to the global value, being brighter by 0.28 ± 0.08 mag.

4. Redshift-space Distortions

A complicating feature of redshift surveys is that the radial distance estimated from the redshift is corrupted by peculiar velocities. Such effects are most readily

https://doi.org/10.1017/S0074180900196524 Published online by Cambridge University Press

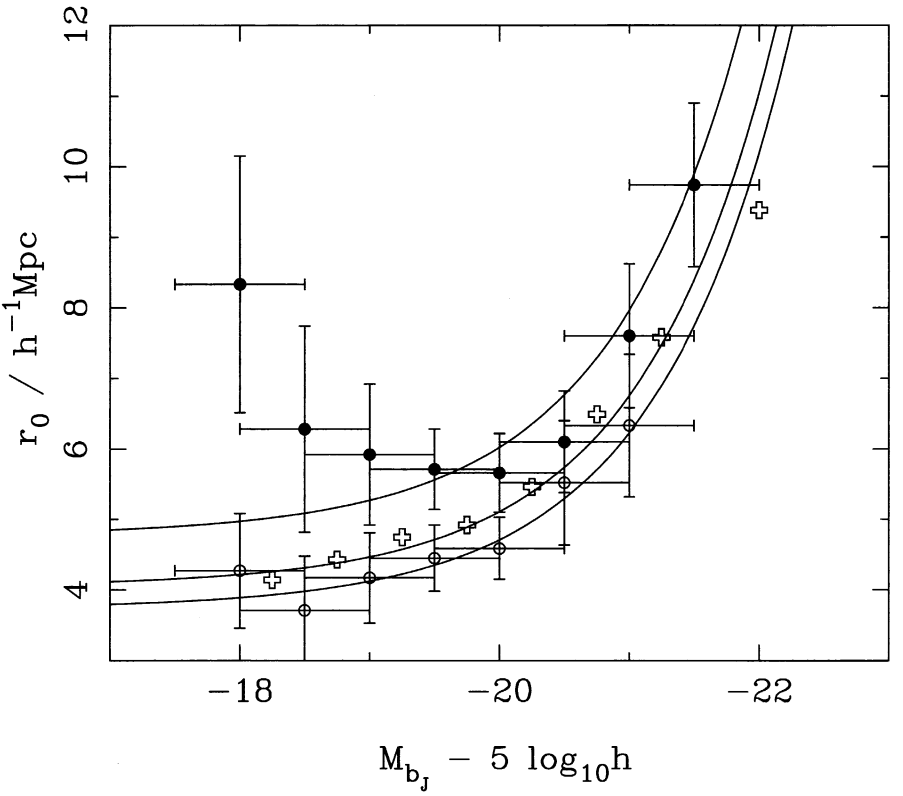

Figure 5. (a) The correlation length in real space as a function of absolute magnitude. Crosses show the results for all galaxies from Norberg et al. (2001); filled and open circles show the early-type / late-type split derived by Norberg et al. (2002). The lines show the fit $b/b^* = 0.85 + 0.15\,(L/L^*)$, with early-type galaxies having a bias 1.16 times larger than the average, and late types a bias 0.93 times smaller. The deviation from this fit for early-type galaxies of the lowest luminosity is intriguing, but this does represent an extremely shallow sample.

measured statistically via the redshift-space correlation function, $\xi(\sigma, \pi)$. This measures the excess probability over random of finding a pair of galaxies with a separation in the plane of the sky σ and a line-of-sight separation π. On small scales the correlation function should be extended in the radial direction due to the large peculiar velocities in non-linear structures such as groups and clusters; on large scales it should be compressed in the radial direction due to the coherent infall of galaxies onto mass concentrations – the Kaiser effect (Kaiser 1987).

The redshift-space correlation function for the 2dFGRS is shown in Figure 6. The correlation-function results display very clearly the two signatures of redshift-space distortions. The 'Fingers of God' from small-scale random velocities are very clear, as indeed has been the case from the first redshift surveys (e.g. Davis & Peebles 1983). The 2dFGRS results were the first to show the large-scale flattening from coherent infall in detail. An initial analysis of this ef-

https://doi.org/10.1017/S0074180900196524 Published online by Cambridge University Press

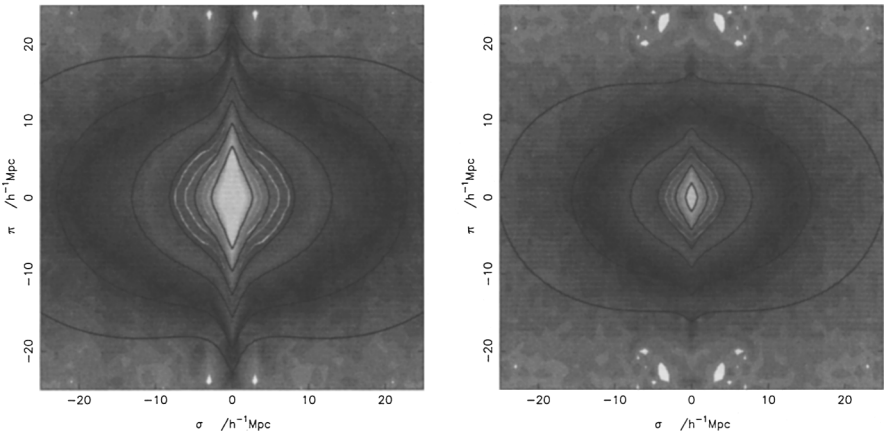

Figure 6. The galaxy correlation function $\xi(\sigma, \pi)$ as a function of transverse (σ) and radial (π) pair separation: early-type (left) and late-type (right). Also plotted are the contour levels of the respective best-fitting models. The contour levels are $\xi = 4.0, 2.0, 1.0, 0.5, 0.2, 0.1$. These diagrams show clearly that early types have both a larger amplitude of clustering and a higher pairwise velocity dispersion. See Madgwick et al. (2003) for details.

fect was performed in Peacock et al. (2001), and the final database was analysed by Hawkins et al. (2003). Redshift-space distortions were analyzed for separate spectral types by Madgwick et al. (2003).

The degree of large-scale flattening is determined by the total mass density parameter, Ω_m, and the biasing of the galaxy distribution. On large scales, it should be correct to assume a linear bias model, with correlation functions $\xi_g(r) = b^2\xi(r)$, so that the redshift-space distortion on large scales depends on the combination $\beta \equiv \Omega_m^{0.6}/b$. This is modified by the Finger-of-God effect, which is significant even at large scales and dominant at small scales. The effect can be modelled by introducing a parameter σ_p, which represents the rms pairwise velocity dispersion of the galaxies in collapsed structures, σ_p (see e.g. Ballinger, Peacock, & Heavens 1996). Considering both these effects, and marginalising over σ_p, the best estimate of β and its 68% confidence interval according to Hawkins et al. (2003) is

$$\beta = 0.49 \pm 0.09 \tag{3}$$

This measurement of $\Omega_m^{0.6}/b$ can only be used to determine Ω_m if the bias is known. We discuss below two methods by which the bias parameter may be inferred, which in fact favour $b \simeq 1$. Some care is needed in this analysis, because the 2dFGRS has a median redshift of 0.11; with weighting, the mean redshift in Hawkins et al. is 0.15, and our measurement should be interpreted as β at that epoch. Optimal weighting also means that the effective mean luminosity is high: it is approximately 1.4 times the characteristic luminosity, L^*, of the overall galaxy population (Folkes et al. 1999; Madgwick et al. 2002).

https://doi.org/10.1017/S0074180900196524 Published online by Cambridge University Press

5. The 2dFGRS Power Spectrum

Perhaps the key aim of the 2dFGRS was to perform an accurate measurement of the 3D clustering power spectrum. The results of direct estimation of the 3D power spectrum are shown in Figure 7 (Percival et al. 2001). This power-spectrum estimate uses the FFT-based approach of Feldman, Kaiser & Peacock (1994), and needs to be interpreted with care. Firstly, it is a raw redshift-space estimate, so that the power beyond $k \simeq 0.2\,h\,\mathrm{Mpc}^{-1}$ is severely damped by Fingers of God. On large scales, the power is enhanced, both by the Kaiser effect and by the luminosity-dependent clustering discussed above. However, Percival, Verde, & Peacock (2004) have shown that luminosity dependence yields no significant distortion of the *shape* of $P(k)$, which is the key point. Finally, the FKP estimator yields the true power convolved with the window function. This modifies the power significantly on large scales (roughly a 20% correction). We have made an approximate correction for this in Figure 7.

The fundamental assumption is that, on large scales, linear biasing applies, so that the nonlinear galaxy power spectrum in redshift space has a shape identical to that of linear theory in real space. We believe that this assumption is valid for $k < 0.15\,h\,\mathrm{Mpc}^{-1}$; the detailed justification comes from analyzing realistic mock data derived from N-body simulations (Cole et al. 1998). The model free parameters are thus the primordial spectral index, n, the Hubble parameter, h, the total matter density, Ω_m, and the baryon fraction, Ω_b/Ω_m. Note that the vacuum energy does not enter. Initially, we show results assuming $n = 1$; this assumption is relaxed later.

An accurate model comparison requires the full covariance matrix of the data, because the convolving effect of the window function causes the power at adjacent k values to be correlated. This covariance matrix was estimated by applying the survey window to a library of Gaussian realisations of linear density fields, and checked against a set of mock catalogues. It is now possible to explore the space of CDM models, and likelihood contours in Ω_b/Ω_m versus $\Omega_m h$ are shown in Figure 8. At each point in this surface we have marginalized by integrating the likelihood surface over the two free parameters, h and the power spectrum amplitude. We have added a Gaussian prior $h = 0.7 \pm 10\%$, representing external constraints such as the HST key project (Freedman et al. 2001); this has only a minor effect on the results.

Figure 8 shows that there is a degeneracy between $\Omega_m h$ and the baryonic fraction Ω_b/Ω_m. However, there are two local maxima in the likelihood, one with $\Omega_m h \simeq 0.2$ and $\sim 20\%$ baryons, plus a secondary solution $\Omega_m h \simeq 0.6$ and $\sim 40\%$ baryons. The high-density model can be rejected through a variety of arguments, and the preferred solution is

$$\Omega_m h = 0.20 \pm 0.03; \qquad \Omega_b/\Omega_m = 0.15 \pm 0.07. \tag{4}$$

A preliminary analysis of $P(k)$ from the full final dataset shows that $P(k)$ becomes smoother: the high-baryon solution becomes disfavoured, and the uncertainties narrow slightly around the lower-density solution: $\Omega_m h = 0.18 \pm 0.02$; $\Omega_b/\Omega_m = 0.17 \pm 0.06$.

It is interesting to compare these conclusions with other constraints. These are shown on Figure 8, assuming $h = 0.7 \pm 10\%$. Estimates of the Deuterium to

https://doi.org/10.1017/S0074180900196524 Published online by Cambridge University Press

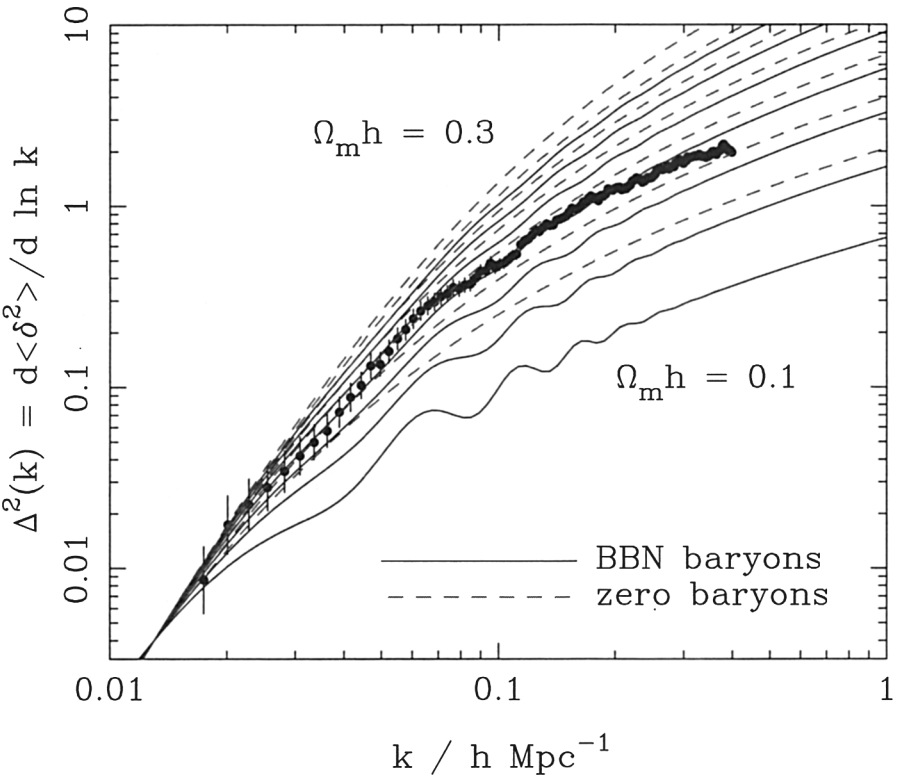

Figure 7. The 2dFGRS redshift-space dimensionless power spectrum, $\Delta^2(k)$, estimated according to the FKP procedure. The solid points with error bars show the power estimate. The window function correlates the results at different k values, and also distorts the large-scale shape of the power spectrum. An approximate correction for the latter effect has been applied. The solid and dashed lines show various CDM models, all assuming $n = 1$. For the case with non-negligible baryon content, a big-bang nucleosynthesis value of $\Omega_b h^2 = 0.02$ is assumed, together with $h = 0.7$. A good fit is clearly obtained for $\Omega_m h \simeq 0.2$. Note that the observed power at large k will be boosted by nonlinear effects, but damped by small-scale random peculiar velocities. It appears that these two effects very nearly cancel, but model fitting is generally performed only at $k < 0.15\,h\,\mathrm{Mpc}^{-1}$ in order to avoid these complications.

Hydrogen ratio in QSO spectra combined with big-bang nucleosynthesis theory predict $\Omega_b h^2 = 0.020 \pm 0.001$ (Burles, Nollett, & Turner 2001), which translates to the shown locus of $f_{\rm B}$ vs $\Omega_m h$. X-ray cluster analysis predicts a baryon fraction $\Omega_b/\Omega_m = 0.127 \pm 0.017$ (Evrard 1997) which is within 1σ of our value. These loci intersect very close to our preferred model.

The main residual worry about accepting the above conclusions is probably whether the assumption of linear bias can really be valid. Until relatively recently, our understanding of bias was sufficiently primitive that it was difficult to remove this worry with certainty. However, a big step forward was taken by

https://doi.org/10.1017/S0074180900196524 Published online by Cambridge University Press

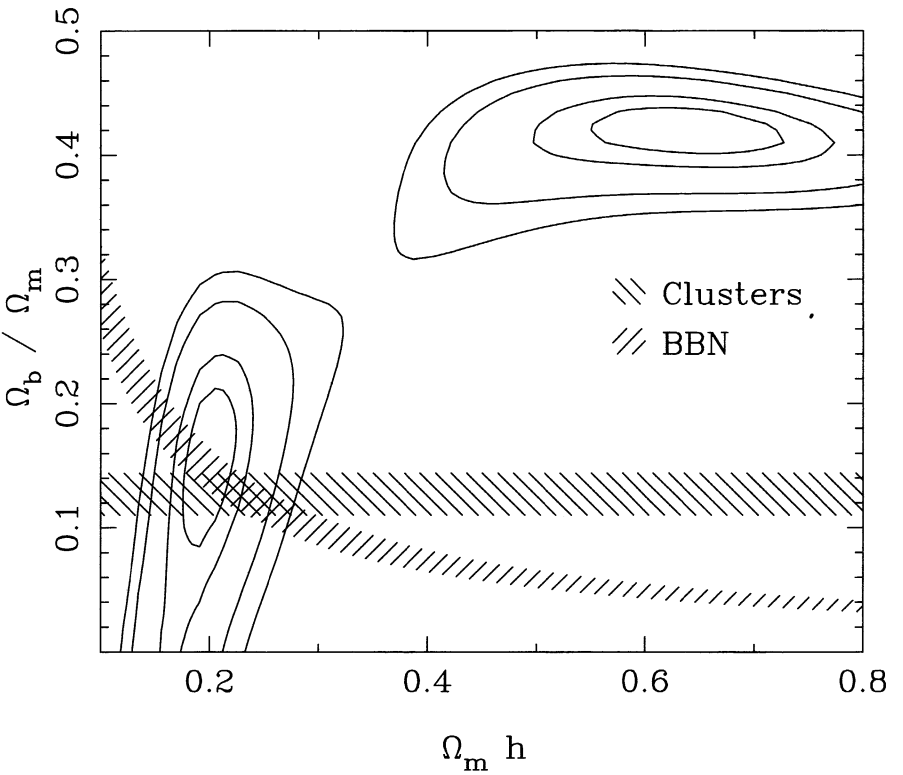

Figure 8. Likelihood contours for the best-fit linear power spectrum over the region $0.02 < k < 0.15$. The normalization is a free parameter to account for the unknown large scale biasing. Contours are plotted at the usual positions for one-parameter confidence of 68%, and two-parameter confidence of 68%, 95% and 99% (i.e. $-2\ln(\mathcal{L}/\mathcal{L}_{\rm max}) = 1, 2.3, 6.0, 9.2$). We have marginalized over the missing free parameters (h and the power spectrum amplitude). A prior on h of $h = 0.7 \pm 10\%$ was assumed. This result is compared to estimates from X-ray cluster analysis (Evrard 1997) and big-bang nucleosynthesis (Burles et al. 2001). A preliminary analysis of the complete final 2dFGRS sample yields a slightly smoother spectrum than the results shown here (from Percival et al. 2001), so that the high-baryon solution becomes disfavoured.

Benson et al. (2000), who showed how a semianalytic model of galaxy formation naturally yielded a correlation function that is close to a single power law over $1000 \gtrsim \xi \gtrsim 1$, even though the mass correlations show a marked curvature over this range. This paper stimulated the analytic 'halo model', which allows one to understand rather simply the differences in shape between the galaxy and mass power spectra (Seljak 2000; Peacock & Smith 2000; Cooray & Sheth 2002). In this approach, the density field is a superposition of dark-matter haloes, with small-scale clustering arising from neighbours in the same halo. It is then possible to demonstrate convincingly that the linear-theory power from the displacement of halo centres should still dominate at the maximum wavenumber of $k = 0.15\,h\,{\rm Mpc}^{-1}$ used by the 2dFGRS.

https://doi.org/10.1017/S0074180900196524 Published online by Cambridge University Press

Despite this theoretical assurance, it is important to test the linear bias assumption directly if possible, and this can be done by considering subsamples with very different degrees of bias. Figure 9 shows the power spectra for the 2dFGRS divided into early and late types by colour. The shapes are almost identical (perhaps not so surprising, since the cosmic variance effects are closely correlated in these co-spatial samples). However, what is impressive is that the relative bias is almost precisely independent of scale, even though the red subset is rather strongly biased relative to the blue subset (relative $b \simeq 1.4$). This provides some reassurance that the large-scale $P(k)$ reflects the underlying properties of the dark matter, rather than depending on the particular class of galaxies used to measure it.

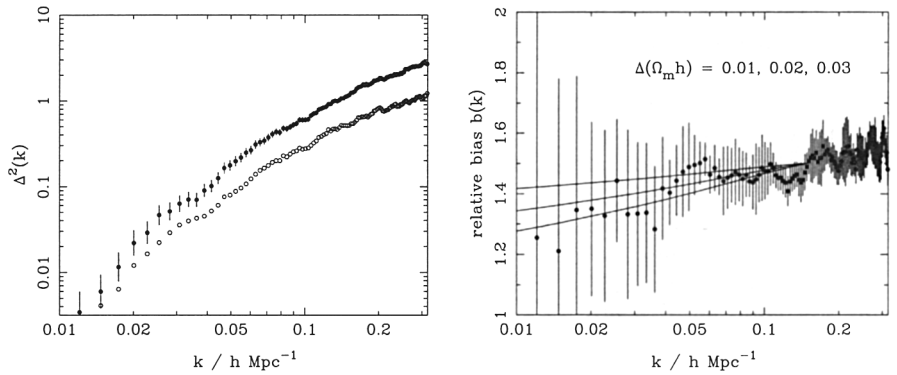

Figure 9. The power spectra of early-type galaxies (filled circles) and late-type galaxies (open circles). The shapes are strikingly similar. The square root of the ratio yields the right-hand panel: the relative bias in redshift space of the two classes. The error bars are obtained by a jack-knife analysis. The relative bias is consistent with a constant value of 1.4 over the range used for fitting of the power-spectrum data ($0.015 < k < 0.15\,h\,\mathrm{Mpc}^{-1}$), although the best-fitting value of $\Omega_m h$ can change by around 1σ depending on which class of galaxy is analysed.

6. Combination with the CMB and Cosmological Parameters

The 2dFGRS power spectrum contains important information about the key parameters of the cosmological model, but we have seen that additional assumptions are needed, in particular the values of n and h. Observations of CMB anisotropies can in principle measure most of the cosmological parameters, and combination with the 2dFGRS can lift most of the degeneracies inherent in the CMB-only analysis. These issues are discussed in Efstathiou et al. (2002) and Percival et al. (2002), and the 2dFGRS played a critical role in the WMAP first-year papers (e.g. Spergel et al. 2003).

The CMB data alone contain two important degeneracies: the 'geometrical' and 'tensor' degeneracies. In the former case, one can evade the commonly-stated CMB conclusion that the universe is flat, by adjusting both Λ and h to extreme values (Zaldarriaga, Spergel, & Seljak 1997; Bond, Efstathiou, &

https://doi.org/10.1017/S0074180900196524 Published online by Cambridge University Press

Tegmark 1997; Efstathiou & Bond 1999). In order to break the degeneracy, additional information is needed. This could be in the form of external data on the Hubble constant, but the most elegant approach is to add the 2dFGRS data, so that conclusions are based only on the shapes of power spectra. Efstathiou et al. (2002) show that doing this yields a total density

$$|\Omega - 1| < 0.05 \tag{5}$$

at 95% confidence. We can therefore be confident that the universe is very nearly flat; hereafter it will be assumed that this is exactly true.

The next most critical question for the CMB is whether the temperature fluctuations are scalar-mode only, or whether there could be a significant tensor signal. The tensor modes lack acoustic peaks, so they reduce the relative amplitude of the main peak at $\ell = 220$. A model with a large tensor component can however be made to resemble a zero-tensor model by applying a large blue tilt ($n > 1$) and a high baryon content. Efstathiou et al. (2002) show that adding the 2dFGRS data weakens this degeneracy, but does not completely remove it. This is reasonable, since the 2dFGRS data alone constrain the baryon content weakly.

The importance of tensors will of course be one of the key questions for cosmology over the next several years, but it is interesting to consider the limit in which these are negligible. In this case, the standard model for structure formation contains a vector of only 6 parameters: $\mathbf{p} = (n_s, \Omega_m, \Omega_b, h, Q, \tau)$. Of these, the optical depth to last scattering, τ, is almost entirely degenerate with the normalization, Q. The remaining four parameters are pinned down very precisely: using a compilation of pre-WMAP CMB data plus the 2dFRGS power spectrum, Percival et al. (2002) obtained

$$\begin{pmatrix} n_s \\ \Omega_c h^2 \\ \Omega_b h^2 \\ h \end{pmatrix} = \begin{pmatrix} 0.963 \pm 0.042 \\ 0.115 \pm 0.009 \\ 0.021 \pm 0.002 \\ 0.665 \pm 0.047 \end{pmatrix}. \tag{6}$$

or an overall density parameter of $\Omega_m = 0.313 \pm 0.055$.

Interestingly, the great improvement in the CMB data by WMAP improves these limits only moderately, with WMAP+2dFGRS yielding

$$\begin{pmatrix} n_s \\ \Omega_c h^2 \\ \Omega_b h^2 \\ h \end{pmatrix} = \begin{pmatrix} 0.97 \pm 0.03 \\ 0.111 \pm 0.006 \\ 0.023 \pm 0.001 \\ 0.73 \pm 0.03 \end{pmatrix} \tag{7}$$

This shows clearly the degeneracy problem: the limiting factor is not so much the CMB data, but what is used in combination. This is of course not to imply that further improvements in the CMB data would be futile – but a very large step in quality will be needed before the CMB alone can break the remaining approximate degeneracies more effectively than can be achieved at present with the aid of external information.

It is striking how well these figures agree with completely independent determinations: $h = 0.72 \pm 0.08$ from the HST key project (Mould et al. 2000;

Freedman et al. 2001); $\Omega_b h^2 = 0.020 \pm 0.001$ (Burles et al. 2001). This gives confidence that the tensor component must indeed be sub-dominant.

Percival et al. (2002) also showed that there is a useful rule of thumb that allows one to see in a direct and simple manner how the CMB and LSS constraints combine. For flat models, there is a degeneracy that is related (but not identical) to the geometrical degeneracy, being very closely related to the location of the acoustic peaks. The angular scale of these peaks depends on the ratio between the horizon size at last scattering and the present-day horizon size for flat models. For matter-dominated models, this would be simply a geometrical factor that depends on Ω_m only. The complication is that radiation is still non-negligible at last scattering, so the 'horizon angle' depends both on Ω_m and on the matter-to-radiation ratio through $\Omega_m h^2$. In practice, the CMB peak multipole number scales approximately as $\ell_{\rm peak} \propto \Omega_m^{-0.14} h^{-0.48}$, i.e. the condition for constant CMB peak location is well approximated as

$$\Omega_m h^{3.4} = \text{constant}. \tag{8}$$

It is now clear how LSS data combines with the CMB: $\Omega_m h^{3.4}$ is measured to very high accuracy already, and Percival et al. (2002) deduced $\Omega_m h^{3.4} = 0.078$ with an error of about 6% using pre-WMAP CMB data. The first-year WMAP results in fact prefer $\Omega_m h^{3.4} = 0.084$ (Spergel et al. 2003); the slight increase arises because WMAP indicates that previous datasets around the peak were, on average, calibrated low.

In any case, the dominant error in Ω_m and h depends on what one chooses to add to the $\Omega_m h^{3.4}$ figure. The best approach given current knowledge is probably to combine the WMAP $\Omega_m h^{3.4} = 0.084$ with the updated 2dFGRS $\Omega_m h = 0.18 \pm 0.02$: this yields $\Omega_m = 0.25 \pm 15\%$ and $h = 0.73 \pm 5\%$.

7. Matter Fluctuation Amplitude and Bias

The above conclusions were obtained by considering the shapes of the CMB and galaxy power spectra. However, it is also of great interest to consider the amplitude of mass fluctuations, since a comparison with the galaxy power spectrum allows us to infer the degree of bias directly. This analysis was performed by Lahav et al. (2002). Given assumed values for the cosmological parameters, the present-day linear normalization of the mass spectrum (e.g. σ_8) can be inferred. It is convenient to define a corresponding measure for the galaxies, $\sigma_{8\rm g}$, such that we can express the bias parameter as

$$b = \frac{\sigma_{8\rm g}}{\sigma_{8\rm m}}. \tag{9}$$

In practice, we define $\sigma_{8\rm g}$ to be the value required to fit a CDM model to the power-spectrum data on linear scales ($0.02 < k < 0.15\,h\,{\rm Mpc}^{-1}$). The amplitude of 2dFGRS galaxies in real space estimated by Lahav et al. (2002) is $\sigma_{8\rm g}^R(L^*) = 0.76$, with a negligibly small random error. This assumes no evolution in $\sigma_{8\rm g}$, plus the luminosity dependence of clustering measured by Norberg et al. (2001).

The value of σ_8 for the dark matter can be deduced from the CMB fits:

$$\sigma_8 = (0.72 \pm 0.04)\,\exp\tau, \tag{10}$$

https://doi.org/10.1017/S0074180900196524 Published online by Cambridge University Press

where the quoted error includes both data errors and theory uncertainty. The WMAP value here is almost identical: $\sigma_8 \exp(-\tau) = 0.71$, but no error is quoted (Spergel et al. 2003). The unsatisfactory feature is the degeneracy with the optical depth to last scattering. For reionization at $z = 8$, we would have $\tau \simeq 0.05$; it is not expected theoretically that τ can be hugely larger, and popular models would place reionization between $z = 10$ and $z = 15$, or $\tau \simeq 0.1$ (e.g. Loeb & Barkana 2001). One of the many impressive aspects of the WMAP results is that they are able to infer $\tau = 0.17 \pm 0.04$ from large-scale polarization. Taken at face value, $\tau = 0.17$ would argue for reionization at $z = 20$, but the error means that more conventional figures are far from being ruled out. Taking all this together, it seems plausible that the true value of σ_8 is within a few % of 0.80. Given the 2dFGRS figure of $\sigma_{8g}^R = 0.76$, this implies that L^* galaxies are very nearly exactly unbiased.

Finally, this conclusion of near-unity bias was reinforced in a completely independent way, by using the measurements of the bispectrum of galaxies in the 2dFGRS (Verde et al. 2002). As it is based on three-point correlations, this statistic is sensitive to the filamentary nature of the galaxy distribution – which is a signature of nonlinear evolution. One can therefore split the degeneracy between the amplitude of dark-matter fluctuations and the amount of bias. At the effective redshift and luminosity of their sample ($z_s = 0.17$ and $L = 1.9L^*$), Verde et al. found $b = 1.04 \pm 0.11$. Although the corrections to zero redshift and to luminosity L^* are probably significant, this reinforces the point that on large scales there is no substantial difference in clustering between typical galaxies and the dark matter (small scales are another matter entirely).

8. Less-standard Ingredients

8.1. Limits to the Neutrino Mass

Even though a CDM-dominated universe matches the data very well, there are many plausible variations to consider. Probably the most interesting is the neutrino mass: oscillation data mean that at least one neutrino must have a mass of $\gtrsim 0.05$ eV, so that $\Omega_\nu \gtrsim 10^{-3}$ – the same order of magnitude as stellar mass. A non-zero neutrino mass can lead to relatively enhanced large-scale power, beyond the neutrino free-streaming scale. Broadly speaking, allowing a significant neutrino mass changes the spectrum in a way that resembles lower density, so there is a near-degeneracy between neutrino mass fraction and $\Omega_m h$. A limit on the neutrino fraction thus requires a prior on $\Omega_m h$. Based on the cluster baryon fraction plus BBN, we adopt $\Omega_m < 0.5$; together with the HST Hubble constant, this yields a marginalized 95% limit of $f_\nu < 0.13$, or $m_\nu < 1.8$ eV (Elgaroy et al. 2002). Note that this is the sum of the eigenvalues of the mass matrix: given neutrino oscillation results, the only way a cosmologically significant density can arise is via a nearly degenerate hierarchy, so this allows us to deduce $m_\nu < 0.6$ eV for any one species. This limit was improved to $m_\nu < 0.23$ eV by the WMAP team, partly owing to the improved limits on Ω_m from the CMB data, but also including a different effect: a non-zero f_ν reduces the CDM growth, and would yield a discrepancy between σ_8 values inferred from the CMB and from LSS.

https://doi.org/10.1017/S0074180900196524 Published online by Cambridge University Press

8.2. The Equation of State of the Vacuum

So far, we have assumed that the vacuum energy is exactly a classical Λ, or at any rate indistinguishable from one. This is a highly reasonable prior: there is no reason for the asymptotic value of any potential to go exactly to zero, so one always needs to solve the classical cosmological constant problem – for which probably the only reasonable explanation is an anthropic one (e.g. Vilenkin 2001). Therefore, dynamical provision of $w \equiv p_v/\rho_v \neq -1$ is not needed. Nevertheless, one can readily take an empirical approach to w (treated as a constant for a first approach).

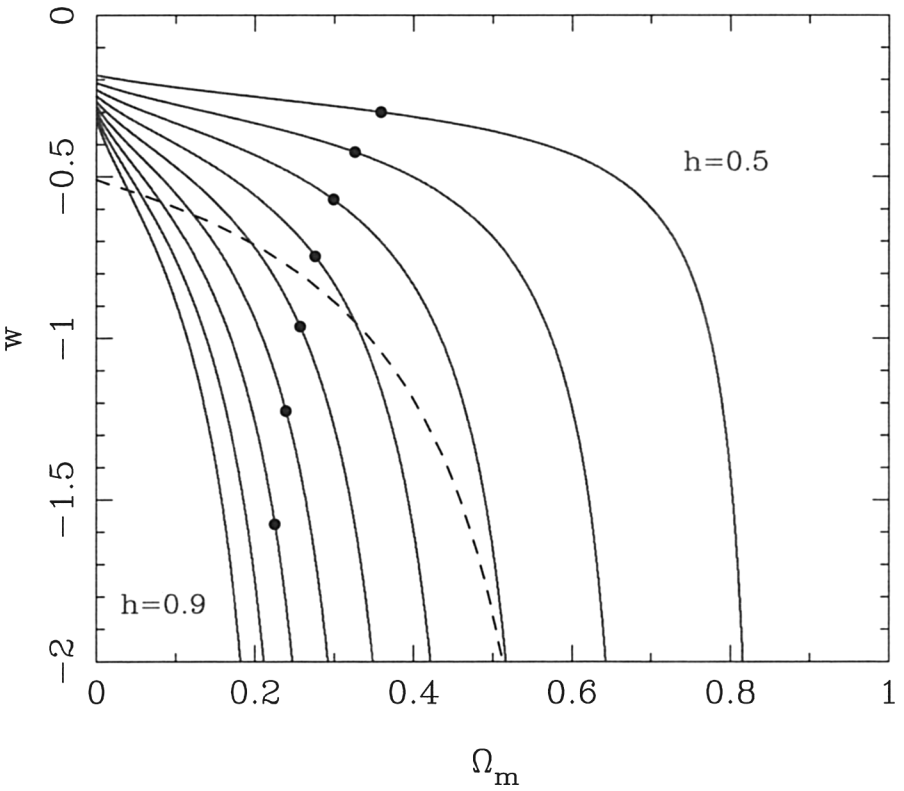

Figure 10. The $\Omega_m h^{3.4}$ degeneracy for flat models gives an almost exact value of Ω_m from the CMB if h is known, assuming the vacuum to be effectively a classical Λ ($w = -1$). If w is allowed to vary, this becomes a locus on the (Ω_m, w) plane (similar to the locus for best-fitting flat models from the SNe, showed dotted). Solid circles show values of $\Omega_m h$ that satisfy the updated 2dFGRS constraint of 0.18 (suppressing error bars).

Figure 10 shows a simplified approach to this, plotting the locus on (w, Ω_m) space that is required for a given value of h if the location of the main CMB acoustic peak is known exactly. The solid circles show the updated 2dFGRS constraint of $\Omega_m h = 0.18$. In order to match the data with w closer to zero, Ω_m must increase and h must decrease. The latter trend means that the HST

https://doi.org/10.1017/S0074180900196524 Published online by Cambridge University Press

Hubble constant sets an upper limit to w of about -0.54 (Percival et al. 2002). This is very similar to the constraints that can be set from SNe Ia. A combined analysis is given by Tonry et al. (2003) and Knop et al. (2003), both groups finding roughly $w = -1.1 \pm 0.2$. The vacuum energy is indeed looking rather similar to Λ.

8.3. The Total Relativistic Density

Finally, an interesting aspect of Figure 10 is that it reminds us of history. When the COBE detection was announced in 1992, a popular model was 'standard' CDM with $\Omega_m = 1$, $h = 0.5$. As we see, this comes close to fitting the CMB data, and such a model is not unattractive in some ways. Can we be sure it is ruled out? Leaving aside the SNe data, one might think to evade the 2dFGRS constraint by altering the total relativistic content of the universe (for example, by the decay of a heavy neutrino after nucleosynthesis). Since 2dFGRS measures the horizon at matter-radiation equality, this will be changed. If the radiation density is arbitrarily boosted by a factor X, the constraint from LSS becomes

$$(\Omega_m h)_{\rm apparent} = X^{-1/2} (\Omega_m h)_{\rm true}. \tag{11}$$

Therefore $X \simeq 8$ is required to allow an Einstein–de Sitter universe.

However, this argument fails, because it does not take into account the effect of the extra radiation on the CMB. As argued above, the location of the acoustic peaks depends on $a_{\rm eq}$, which depends on ω_m. However, if we change the radiation content, then what matters is ω_m/X. Thus, the CMB peak constraint now reads

$$\Omega_m^{-0.1} (\omega_m/X)^{0.24} = \text{constant}; \tag{12}$$

when combining LSS and CMB, everything is as before except that the effective Hubble parameter is $h/X^{1/2}$. Thus, a model with $\Omega_m = 1$ but boosted radiation would only fit the CMB with $h \simeq 0.5\sqrt{8} \simeq 1.4$, and the attractiveness of a low age is lost. In any case, combining LSS and CMB would give the same $\Omega_m \simeq 0.3$ independent of X, so it is impossible to save models with $\Omega_m = 1$ by this route.

Finally, it is interesting to invert this argument. Since Percival et al. (2002) obtain an effective h of 0.665 ± 0.047 and Freedman et al. (2001) measure $h = 0.72 \pm 0.08$, we deduce

$$1.68X = 1.82 \pm 0.24. \tag{13}$$

This convincingly rules out the $1.68X = 1$ that would apply if the universe contained only photons, and amounts to a detection of the neutrino background. In terms of the number of neutrino species, this is $N_\nu = 3.6 \pm 1.1$. A more precise result is of course obtained from primordial nucleosynthesis, but this applies at a much later epoch, thus constraining models with decaying particles.

9. Conclusions

The 2dFGRS is the first 3D survey of the local universe to achieve 100,000 redshifts, almost an order of magnitude improvement on previous work. See

https://doi.org/10.1017/S0074180900196524 Published online by Cambridge University Press

`http://www.mso.anu.edu.au/2dFGRS/Public` for details of the 2dFGRS. In particular, this site gives details of the 2dFGRS public data release.

Overall, these beautiful results on the large-scale structure of the universe, plus the incredible recent progress in CMB data have defined a very clear 'standard model' for structure formation. This consists of a scalar-mode adiabatic CDM universe with scale-invariant fluctuations. Measuring the exact parameters of this model is rendered difficult by the intrinsic degeneracies of the structure-formation process, but progress is being made. The most recent data yield $\Omega_m = 0.25 \pm 15\%$ and $h = 0.73 \pm 5\%$; these figures accord well with independent constraints, and it is very hard to believe that they are incorrect.

Allowing extra degrees of freedom, such as massive neutrinos, vacuum equation of state $w \neq 1$, or extra relativistic content worsens the agreement with independent constraints on h and Ω_m. This both supports the simplest picture and allows us to set interesting limits on these non-standard ingredients.

Despite these achievements, there remains much to look forward to. The great target in fundamental physics is to test inflation: the current data are consistent with $n = 1$ to an error of ± 0.03. Once this is halved, plausible levels of tilt will come within our sensitivity. The tensor fraction is a less clear target, but the motivation to improve on the current weak upper limits will remain strong. However, it is clear that these next steps will be demanding: it will be necessary to understand in some detail differences in the distribution of mass and light in the universe. Fortunately, this is an astrophysical challenge that is of great interest in its own right.

Acknowledgments. The 2dF Galaxy Redshift Survey was made possible by the dedicated efforts of the staff of the Anglo-Australian Observatory, both in creating the 2dF instrument, and in supporting it on the telescope.

References

Ballinger, W. E., Peacock, J. A., & Heavens, A. F. 1996, MNRAS, 282, 877
Benoist, C., Maurogordato, S., da Costa, L. N., Cappi, A., & Schaeffer, R. 1996, ApJ, 472, 452
Benson, A. J., Cole, S., Frenk, C. S., Baugh, C. M., & Lacey C. G. 2000, MNRAS, 311, 793
Bond, J. R., Efstathiou, G., & Tegmark, M. 1997, MNRAS, 291, L33
Burles, S., Nollett, K. M., & Turner, M. S. 2001, ApJ, 552, L1
Cole, S., Hatton, S., Weinberg D. H., & Frenk C. S. 1998, MNRAS, 300, 945
Cole, S., & Kaiser, N. 1989, MNRAS, 237, 1127
Colless, M., et al. 2001, MNRAS, 328, 1039
Colless, M., et al. 2003, astro-ph/0306581
Cooray, A., & Sheth, R. 2002, Physics Reports, 372, 1
Davis, M., & Geller, M. J. 1976, ApJ, 208, 13
Davis, M., & Peebles, P. J. E. 1983, ApJ, 267, 465
De Propris, R., et al. 2003, MNRAS, 342, 725
Efstathiou, G., & Bond J. R. 1999, MNRAS, 304, 75
Efstathiou, G., et al. 2002, MNRAS, 330, L29
Elgaroy, O., et al. 2002, Phys.Rev.Lett, 89, 061301

Evrard, A. 1997, MNRAS, 292, 289
Folkes, S. J., et al. 1999, MNRAS, 308, 459
Feldman, H. A., Kaiser, N., & Peacock, J. A. 1994, ApJ, 426, 23
Freedman, W. L., et al. 2001, ApJ, 553, 47
Hambly, N. C., Irwin, M. J., MacGillivray, H. T. 2001, MNRAS 326, 1295
Hawkins, E. J., et al. 2003, MNRAS, 346, 78
Kaiser, N. 1987, MNRAS, 227, 1
Kauffmann, G., Nusser, A., & Steinmetz, M. 1997, MNRAS, 286, 795
Knop, R. A. et al. 2003, ApJ, 598, 102
Lahav, O., et al. 2002, MNRAS, 333, 961
Lewis, I. J., et al. 2002, MNRAS, 333, 279
Loeb, A., & Barkana, R. 2001, ARAA, 39, 19
Loveday, J., Maddox, S. J., Efstathiou, G., & Peterson, B. A. 1995, ApJ, 442, 457
Maddox, S. J., Efstathiou, G., & Sutherland, W. J. 1990c, MNRAS, 246, 433
Maddox, S. J., Efstathiou, G., Sutherland, W. J., & Loveday, J. 1990a, MNRAS, 242, 43P
Maddox, S. J., Sutherland, W. J., Efstathiou, G., & Loveday, J. 1990b, MNRAS, 243, 692
Madgwick, D., et al. 2002, MNRAS, 333, 133
Madgwick, D., et al. 2003, MNRAS, 344, 847
Mo, H. J., & White, S. D. M. 1996, MNRAS, 282, 347
Mould, J. R., et al. 2000, ApJ, 529, 786
Norberg, P., et al. 2001, MNRAS, 328, 64
Norberg, P., et al. 2002, MNRAS, 332, 827
Peacock, J. A., & Smith, R. E. 2000, MNRAS, 318, 1144
Peacock, J. A., et al. 2001, Nature, 410, 169
Percival, W. J., et al. 2001, MNRAS, 327, 1297
Percival, W. J., et al. 2002, MNRAS, 337, 1068
Percival, W. J., Verde, L., & Peacock, J. A. 2004, MNRAS, 347, 645
Schlegel, D. J., Finkbeiner, D. P., & Davis, M. 1998, ApJ, 500, 525
Seljak, U. 2000, MNRAS, 318, 203
Spergel, D. N., et al. 2003, ApJS, 148, 175
Stoughton, C. L., et al. 2002, AJ, 123, 485
Tonry, J. L., et al. 2003, ApJ, 594, 1
Verde, L., et al. 2002, MNRAS, 335, 432
Vilenkin, A. 2003, in STScI Symp. Ser. Vol. 15, The Dark Matter Universe: Matter, Energy and Gravity, ed. M. Livio (Cambridge: Cambridge University Press), 173, hep-th/0106083
Zaldarriaga, M., Spergel, D., & Seljak, U. 1997, ApJ, 488, 1